Supporting Information

Ohhashi et al. 10.1073/pnas.1715483115

SI Methods

Yeast Strains. We used isogenic [*psi*$^-$][*PIN*$^+$] and [*PSI*$^+$] derivatives of the 74D-694 yeast strain (1). [*PSI*$^+$(WT-4)] and [*PSI*$^+$(WT-37)] strains were generated by infection of [*psi*$^-$] yeast with in vitro-generated Sup35NM WT-4 and WT-37 amyloid formed at 4 °C and 37 °C, respectively (1). [*PSI*$^+$(S17R)] strains were generated by overexpression of the Sup35NM S17R mutant with a C-terminal GFP tag or introduction of in vitro-generated Sup35-NM S17R amyloid in [*psi*$^-$] yeast. Both the overexpression and infection experiments induced similar weak/sectoring phenotypes of [*PSI*$^+$(S17R)] strains.

Plasmid Construction. For bacterial expression of Sup35NM, pAED4, or pET29b vectors including a C-terminal 7× histidine-tag were used (1–3). Mutations were introduced by site-directed mutagenesis (Takara Bio.) and confirmed by DNA sequencing.

Expression and Purification of Sup35NM Protein. Nonlabeled and uniformly ^{15}N-labeled Sup35NM was overexpressed in the bacterial strain Rosetta (DE3) and purified by nickel-nitrilotriacetic acid histidine-tag affinity chromatography and cation-exchange chromatography under denaturing conditions as previously reported (1–3). For purification of cysteine mutants, 5 mM 2-mercaptoethanol was added to the buffer. Uniformly ^{2}H,^{15}N-labeled Sup35NM was overexpressed in Spectra 9 medium (Cambridge Isotope Laboratories, Inc.) and purified in the same manner. The Sup35NM protein was desalted by reverse-phase HPLC chromatography (Hitachi) using a Protein-R column (Nacalai Tesque) followed by lyophilization.

Mass Spectral Analysis of Amyloid Core. G2 or the G3 amyloid was treated with proteinase K (0.15 mg/mL) for 1 h at room temperature (4, 5). Proteinase K-resistant amyloid fibers were collected by ultracentrifugation (154,000 × *g* for 30 min), and the pellets were dissolved in 6 M guanidine hydrochloride, 10 mM Tris·HCl (pH 7.5). The dissociated amyloid core peptides were desalted by NuTip C-4 or C-18 (Glygen Corporation) and analyzed by MALDI-TOF-MS (microflex, Bruker Daltonics) and MALDI-TOF/TOF-MS (4800 Plus MALDI TOF/TOF Analyzer, AB SCIEX) for mass spectral analysis of high and low molecular weight regions, respectively. MS spectra were calibrated by bovine ubiquitin. High molecular weight MS data were analyzed using PAWS software (ProteoMetrics).

T_m Analysis. Freshly prepared Sup35NM G2 amyloid was used at concentration of 5 μM in buffer C including 1% SDS that inhibits reaggregation of dissociated proteins. The thermal disassembly of amyloids was examined by the temperature-scanning mode of CD spectroscopy (J-818 Spectropolarimeter; JASCO) at the wavelength of 220 nm. Data were fitted by sigmoidal curve, and T_m values were determined as reported previously (1). Before and after the T_m measurement experiments, CD spectra of Sup35NM from 200–250 nm were acquired at 25 and 95 °C.

Amyloid Infection. Infection of [*psi*$^-$] yeast with in vitro-generated Sup35NM amyloid fibers was performed as previously reported (1).

NMR Backbone Signal Assignment. Backbone resonances of Sup35NM were assigned sequence specifically by analyzing 3D HN(CO)CA, HNCA, CBCANH, CBCA(CO)NH, HN(CA)CO, HNCO, and HN(CA)NNH as previously reported (6, 7). These spectra were acquired with a Bruker Avance III 800 spectrometer equipped with a cryogenic probe at 25 °C. To avoid protein aggregation, these spectra were measured in 50 mM Mes buffer including 10% D_2O (pH 3.0). After the assignment, signals were traced by pH titration measurement from pH 3.0 to pH 5.2. NMR data were processed by TopSpin (Bruker BioSpin) or XWINNMR (Bruker BioSpin) and analyzed by SPARKY (https://www.cgl.ucsf.edu/home/sparky). Ninety-four percent of the signals of main-chain amide protons were successfully assigned. A Sup35NM solution was passed through a 100-kDa-cutoff filter before NMR measurement for elimination of preexisting aggregates. Details are described below.

T_1 and T_2 and NOE Analysis. NMR relaxation measurements of 100 μM Sup35NM were performed in 50 mM Mes buffer (pH 5.2) at 37 °C with a Bruker Avance III 600 spectrometer equipped with a cryogenic probe. The relaxation delay for T_1 and T_2 measurements was 3 s. The ^{15}N T_1 and ^{15}N T_2 decays were recorded using 10 data points: 0.010, 0.050, 0.100, 0.200, 0.300, 0.400, 0.600, 0.800, 1.000, and 1.400 s and 0.017, 0.034, 0.051, 0.068, 0.085, 0.102, 0.136, 0.170, 0.204, and 0.238 s, respectively. ^{1}H-^{15}N heteronuclear NOE values were measured with two different datasets, one collected without initial proton saturation and a second one with initial proton saturation (8).

CLEANEX-PM NMR Analysis. CLEANEX-PM measurements of 100 μM Sup35NM were performed in 50 mM Mes buffer (pH 5.2) at 37 °C with a Bruker Avance III 600 spectrometer equipped with a cryogenic probe. The ^{1}H-^{15}N signal recovery by proton exchange with bulk solvent was recorded using five different mixing times (10, 20, 35, 50, and 65 ms). The hydrogen exchange rate, k_{ex}, was determined by single exponential fitting of the data using Igor software (Wavemetrics).

STD NMR Analysis. ^{1}H-^{15}N STD-HSQC spectra were recorded using a Bruker Avance 500 spectrometer equipped with a cryogenic probe. Measurements were performed with an equal mixture of nonlabeled Sup35NM and uniformly ^{2}H,^{15}N-labeled Sup35NM (total 100 μM Sup35NM in the mixture) in 50 mM Mes (pH 5.2) including 10% D_2O at 22 °C. To exclude water-edited pseudosignals, STD signals of only ^{2}H,^{15}N-labeled Sup35NM were used as a control. STD-HSQC spectra were acquired with selective methyl proton irradiation of nonlabeled Sup35NM at 3 ppm for on-resonance spectra and at 40 ppm for off-resonance reference spectra (9). The irradiation power level was 60 db, and the saturation time was 3 s.

PRE NMR Analysis. After 2-mercaptoethanol was eliminated by dilution and the Sup35NM protein solution was reconsitituted, the single-cysteine mutant was treated with a 10-fold excess of MTSL (Toronto Research Chemicals, Inc.) in 6 M guanidium hydrochloride at room temperature for 2 h. MTSL-labeled Sup35NM was desalted by reverse-phase HPLC chromatography (Protein-R; Nacalai Tesque), followed by lyophilization. PRE effects were monitored by ^{1}H-^{15}N HSQC signal intensity on a Bruker Avance III 600 spectrometer equipped with a cryogenic probe. ^{15}N-labeled/MTSL-labeled Sup35NM spectra reflect the inter- and intramolecular PRE effects, while the ^{14}N-nonlabeled/MTSL-labeled Sup35NM and ^{15}N-free/MTSL-free Sup35NM spectra reflect only intermolecular PRE effects (10).

Amyloid Formation Kinetics Probed by ThT. Spontaneous and seeded amyloid formation kinetics were monitored with a plate reader (Spectra Max M2; Molecular Devices), using ThT (Sigma) as a

fluorescent probe (3). Excitation of ThT fluorescence was at 442 nm, and emission was monitored at 485 nm. Typical reactions include 5 μM Sup35NM and 20 μM ThT in 5 mM buffer C in the absence or presence of sonicated preformed amyloids as seeds [5% (mol/mol)].

Solid-State NMR Analysis. Solid-state NMR experiments on Sup35NM fibrils, where all four Phe residues were labeled by Phe-1-^{13}C, were carried out using a Varian INOVA spectrometer operating at 14.1 Tesla (600 MHz) and a 1.6 mm FAST-MAS probe. All datasets were recorded at an MAS frequency of 20 kHz and a sample temperature of 15 °C. Dipolar dephasing was achieved by PITHIRDS-CT recoupling as described by Tycko et al. (11). Pulse lengths of the 180° pulses for fpRFDR recoupling and PITHIRDS constant time blocks were equal to one-third of the rotor period, τ_R, i.e., 16.67 μs. Amplitudes of the 180° pulses were calibrated from a ^{13}C CP (cross polarization) followed by a 270° pulse of the length of 25 μs. The dipolar recoupling period, τ'_D, was incremented by a rearrangement of pulses within the recoupling sequence, which was incremented from 0–48 ms in steps of 4.8 ms. Each PITHIRDS-CT data point was obtained by adding 1,024 scans, with a recycle delay of 2 s. PITHIRDS-CT reference dephasing curves were calculated with the SIMPSON program using a linear five-spin system with internuclear distances from 4 Å to 8 Å. The raw PITHIRDS-CT data, $S_{raw}(t)$ were corrected for the 1.1% natural abundance of ^{13}C, which was estimated as a roughly linear decay of the signal to 70% after 68 ms (12, 13). The corrected decay curve, $S_{cor}(t)$, was calculated with the following equation: $S_{cor}(t) = [S_{raw}(t) - f_{na}(100 - 0.39 \times t/\text{ms})]/(1 - f_{na})$, where $f_{na,}$ the fraction of the ^{13}C signal due to the natural abundance spins, was estimated as 0.4 assuming that in a dry sample all ^{13}C′ spins contribute in a similar way to the CP signal, and $S_{raw}(t)$ was scaled such that $S_{raw}(0) = 100$.

CD Spectra. CD spectra of Sup35NM monomer were acquired at 37 °C with a J-818 Spectropolarimeter (Jasco) equipped with a Peltier thermal controller as previously reported (14).

Analytical Ultracentrifugation. Velocity area under the curve experiments were performed in a Beckman Optima XL-I analytical ultracentrifuge using an An60Ti rotor at 37 °C, and data were analyzed with Sedfit using the *c(S)* distribution method (www.analyticalultracentrifugation.com) as previously reported (14).

SDD-AGE. Yeast cells were grown in yeast extract/peptone/dextrose liquid medium for 1 d, collected, and resuspended in lysis buffer [25 mM Tris, 100 mM NaCl, 10 mM $MgCl_2$, 1 mM DTT, 5% glycerol, 1 mM EDTA, 1 mM PMSF, Protease Inhibitor mixture (pH 7.5)]. Cells were broken by a Multi Beads Shocker (Yasui Kikai), and lysates were cleared by brief centrifugation. Yeast lysates mixed with sample buffer (final 2% SDS) and run on a 1.5% agarose gel. Proteins were transferred to PVDF membranes (Millipore) and probed with an anti-Sup35 polyclonal antibody (14).

1. Tanaka M, Chien P, Naber N, Cooke R, Weissman JS (2004) Conformational variations in an infectious protein determine prion strain differences. *Nature* 428:323–328.
2. Tanaka M, Collins SR, Toyama BH, Weissman JS (2006) The physical basis of how prion conformations determine strain phenotypes. *Nature* 442:585–589.
3. Chien P, DePace AH, Collins SR, Weissman JS (2003) Generation of prion transmission barriers by mutational control of amyloid conformations. *Nature* 424:948–951.
4. Smirnovas V, et al. (2009) Distinct structures of scrapie prion protein (PrPSc)-seeded versus spontaneous recombinant prion protein fibrils revealed by hydrogen/deuterium exchange. *J Biol Chem* 284:24233–24241.
5. Furukawa Y, Kaneko K, Yamanaka K, Nukina N (2010) Mutation-dependent polymorphism of Cu,Zn-superoxide dismutase aggregates in the familial form of amyotrophic lateral sclerosis. *J Biol Chem* 285:22221–22231.
6. Ikura M, Kay LE, Bax A (1990) A novel approach for sequential assignment of 1H, 13C, and 15N spectra of proteins: Heteronuclear triple-resonance three-dimensional NMR spectroscopy. Application to calmodulin. *Biochemistry* 29:4659–4667.
7. Kay LE, Ikura M, Tschudin R, Bax A (1990) Three-dimensional triple-resonance NMR spectroscopy of isotopically enriched proteins. *J Magn Reson* 89:496–514.
8. Farrow NA, et al. (1994) Backbone dynamics of a free and phosphopeptide-complexed Src homology 2 domain studied by 15N NMR relaxation. *Biochemistry* 33:5984–6003.
9. Mayer M, Meyer B (2001) Group epitope mapping by saturation transfer difference NMR to identify segments of a ligand in direct contact with a protein receptor. *J Am Chem Soc* 123:6108–6117.
10. Clore GM, Iwahara J (2009) Theory, practice, and applications of paramagnetic relaxation enhancement for the characterization of transient low-population states of biological macromolecules and their complexes. *Chem Rev* 109:4108–4139.
11. Tycko R (2007) Symmetry-based constant-time homonuclear dipolar recoupling in solid state NMR. *J Chem Phys* 126:064506.
12. Shewmaker F, Kryndushkin D, Chen B, Tycko R, Wickner RB (2009) Two prion variants of Sup35p have in-register parallel beta-sheet structures, independent of hydration. *Biochemistry* 48:5074–5082.
13. Shewmaker F, Wickner RB, Tycko R (2006) Amyloid of the prion domain of Sup35p has an in-register parallel beta-sheet structure. *Proc Natl Acad Sci USA* 103:19754–19759.
14. Ohhashi Y, Ito K, Toyama BH, Weissman JS, Tanaka M (2010) Differences in prion strain conformations result from non-native interactions in a nucleus. *Nat Chem Biol* 6:225–230.

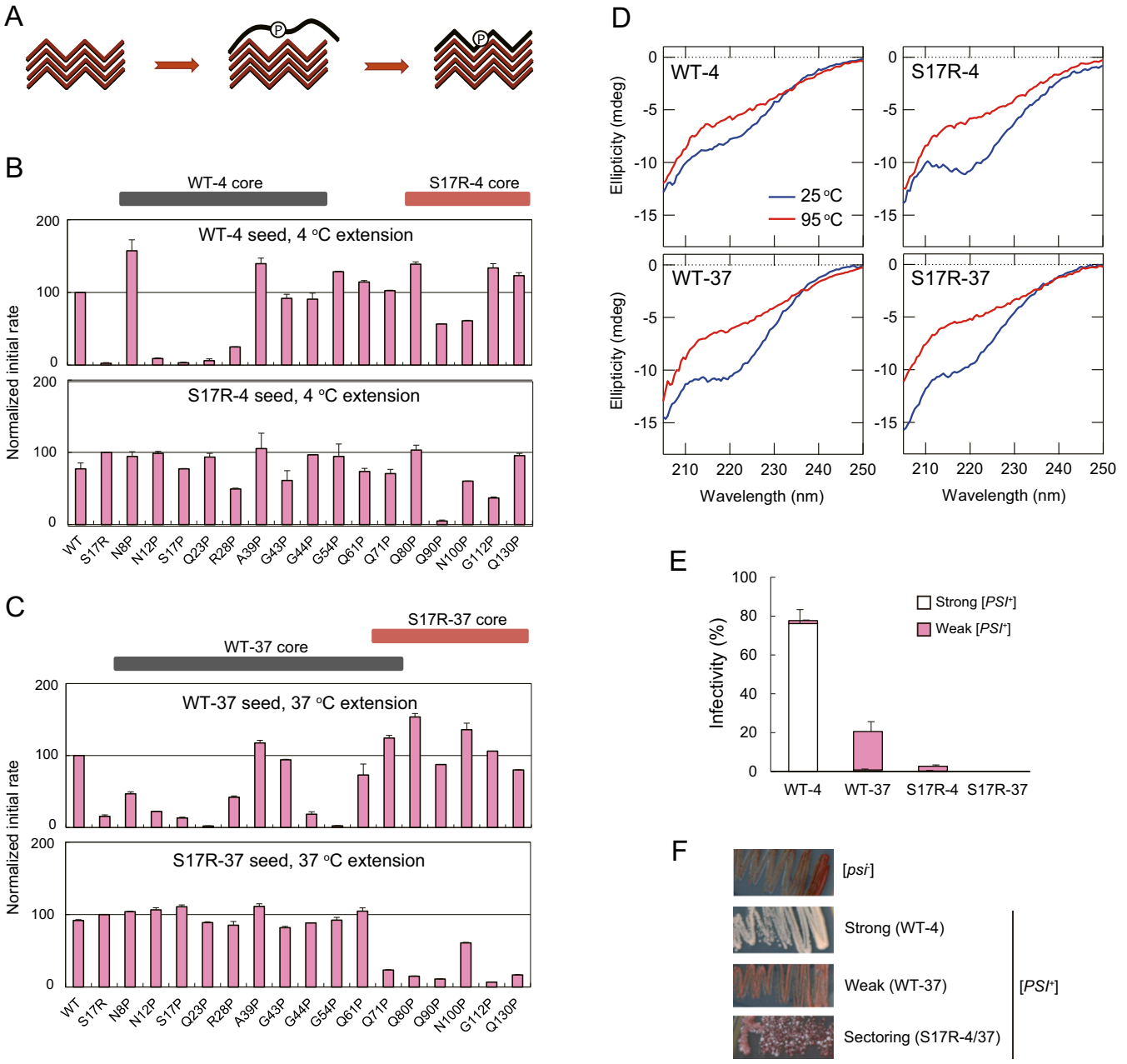

Fig. S1. Sup35NM can form two strikingly distinct amyloid conformations. (*A*) Schematic representation of proline-scanning experiments. The proline (P) mutation, which is located in the region critical to the monomer binding to amyloid seeds, causes defects in the initial rates of seeding reactions. (*B*) Initial rates of seeding reactions of 16 selected proline mutants monitored by ThT fluorescence using WT-4 and S17R-4 amyloid seeds. Initial rates were calculated by linear fitting of an increase in ThT fluorescent intensity, and the resulting values were normalized to the rate of seeding reactions using WT or S17R Sup35NM monomers with WT or S17R amyloid seeds, respectively. Gray and red bars indicate the core regions of WT-4 and S17R-4 amyloids, respectively. (*C*) Initial rates of seeding reactions of 16 selected proline mutants monitored by ThT fluorescence using WT-37 and S17R-37 amyloid seeds. Gray and red bars indicate the core regions of WT-37 and S17R-37 amyloids, respectively. The initial rates are an average from two independent experiments. Error bars denote SEM. (*D*) Far-UV CD spectra of WT-4, WT-37, S17R-4, and S17R-37 amyloids at 25 °C (blue) and 95 °C (red) in the T_m experiments. (*E*) Infectivity of in vitro-generated Sup35NM amyloids and prion strains obtained by protein infection to [*psi*$^-$] yeast. The S17R amyloid shows very low infectivity. White and pink bars indicate strong and weak/sectoring phenotypes, respectively. The infectivity is an average from four independent experiments. Error bars denote SEM. (*F*) Color phenotypes of prion strains obtained by infection with Sup35NM amyloid. WT-4 and WT-37 amyloids induce the stable white (strong) and pink (weak) [*PSI*$^+$] phenotypes, respectively, while S17R amyloid caused unstable sectoring/weak [*PSI*$^+$] phenotypes.

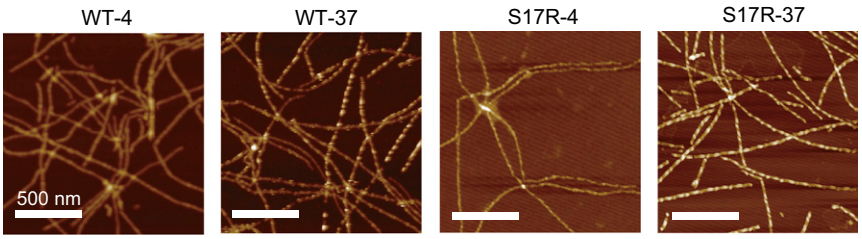

Fig. S2. AFM images of WT and S17R Sup35NM amyloids.

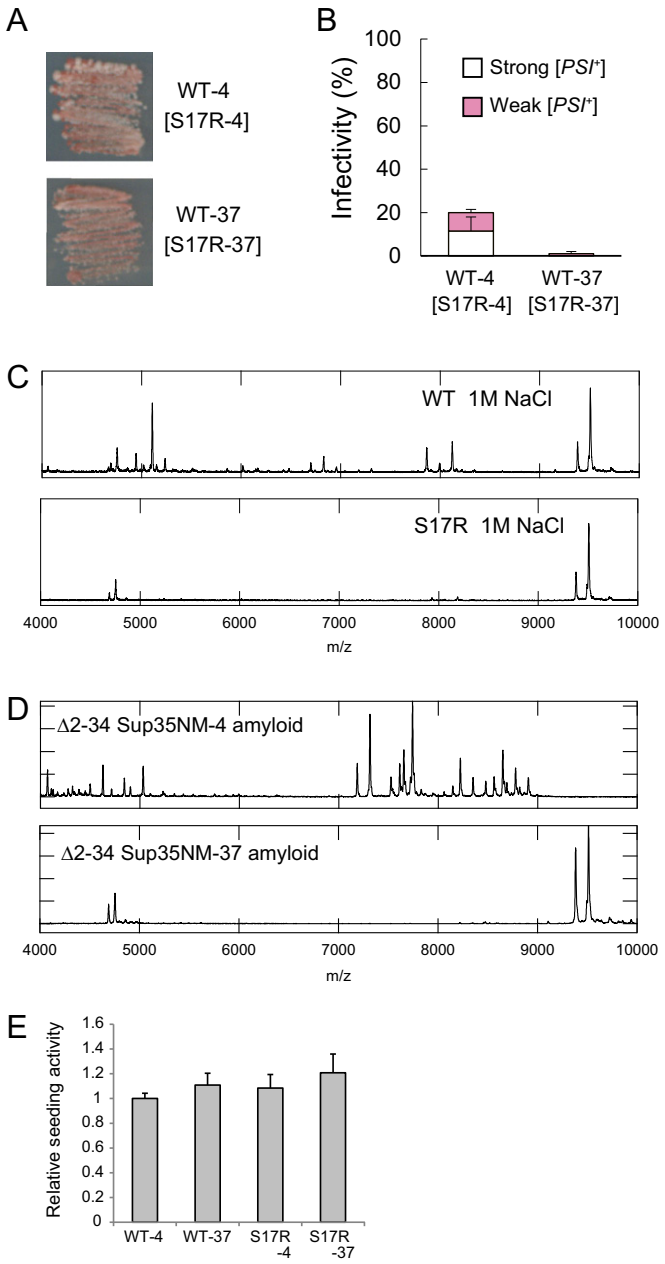

Fig. S3. WT Sup35NM has the potential to form a PrD-C core. (*A*) Typical color phenotypes of [*PSI*$^{+}$(WT[S17R])] strains obtained by infection of [*psi*$^{-}$] yeast by in vitro-generated WT[S17R] amyloid. (*B*) Infectivity of Sup35NM amyloids and color phenotypes of prion strains obtained by protein infection of [*psi*$^{-}$] yeast. White and pink bars indicate strong and weak/sectoring phenotypes, respectively. The infectivity is an average from two independent experiments. Error bars denote SEM. (*C*) High-*m/z*-range MALDI-TOF-MS spectra (*m/z* 4,000–10,000) of core peptides derived from Sup35NM WT (*Upper*) and S17R (*Lower*) amyloids formed in the presence of 1 M NaCl in buffer C at 37 °C. Note that the peptides (amino acids 61/62–144) of the S17R-type amyloid core were detected in both mass spectra. (*D*) High-*m/z*-range MALDI-TOF-MS spectra (*m/z* 4,000–10,000) of core peptides derived from Δ2–34 Sup35NM-4 (*Upper*) and Δ2–34 Sup35NM-37 (*Lower*) amyloids. (*E*) Seeding activity of WT and S17R amyloids toward the WT monomer. The normalized seeding activity at 30 °C is an average from four independent experiments. Error bars denote SEM; $n = 4$.

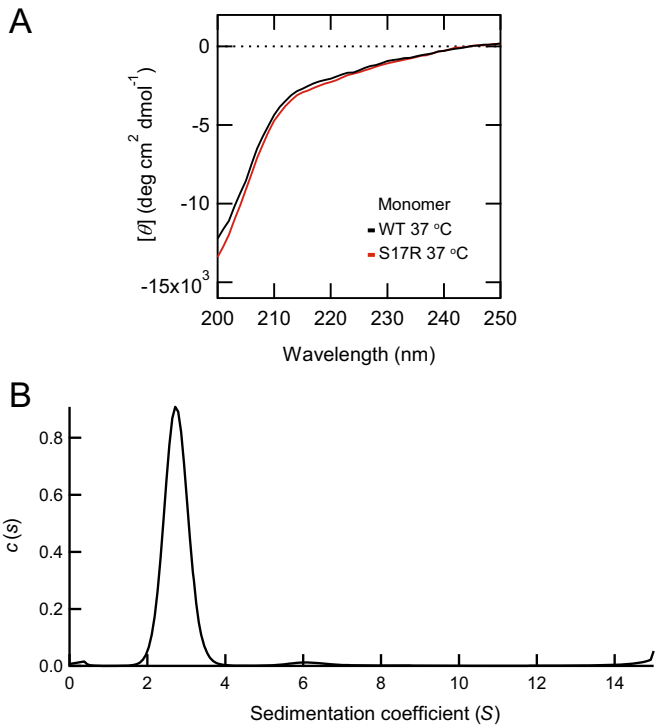

Fig. S4. Sup35NM is an intrinsically disordered monomeric protein at 37 °C. (*A*) Far-UV CD spectra of WT (black) and S17R (red) monomer Sup35NM at 37 °C. (*B*) Distribution of sedimentation coefficients of WT Sup35NM monomer (100 μM) at pH 5.3 and 37 °C by analytical ultracentrifugation.

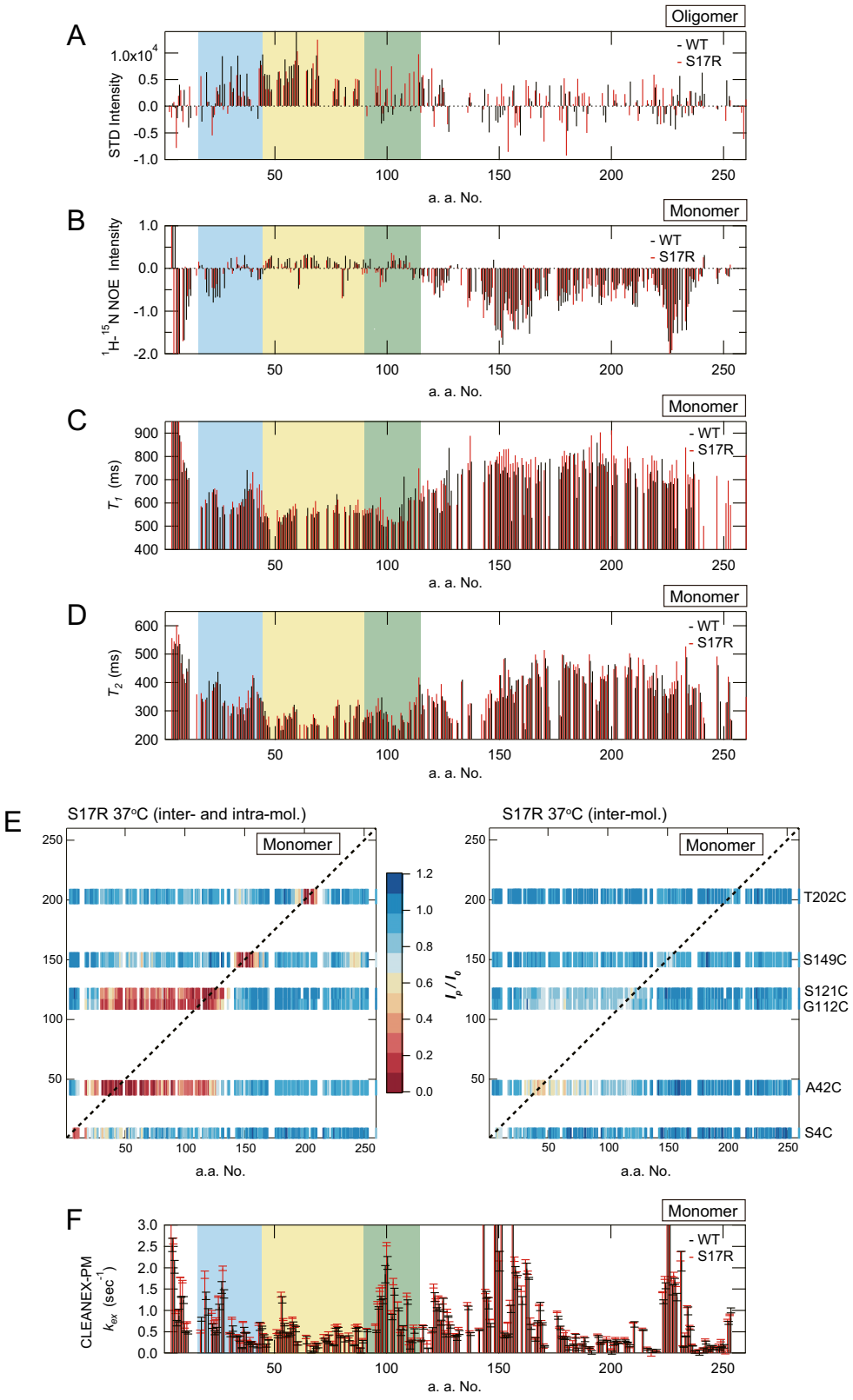

Fig. S5. Intrinsically disordered Sup35NM protein forms latent compact local structures. (*A*) STD signal intensity of WT (black) and S17R (red) Sup35NM at 22 °C. The blue and green areas indicate the amino acid regions with increased STD signals specific to WT and S17R Sup35NM, respectively. (*B*) ^{1}H-^{15}N heteronuclear NOE values for WT (black) and S17R (red) Sup35NM at 37 °C. (*C*) ^{15}N longitudinal relaxation times (T_1) of WT (black) and S17R (red) Sup35NM monomers at 37 °C. (*D*) ^{15}N transverse relaxation times (T_2) of WT (black) and S17R (red) Sup35NM monomers at 37 °C. (*E*) PRE of the S17R Sup35NM monomer monitored by ^{1}H-^{15}N HSQC signal intensity. A MTSL spin probe was introduced into each selected single-cysteine Sup35NM mutant (S4C, A42C, G112C, S121C, S149C, and T202C). Inter/intramolecular (*Left*) and intermolecular (*Right*) PRE values at 37 °C are shown as a color scale showing the I_p/I_0 ratio. (*F*) Hydrogen exchange rates of WT (black) and S17R (red) Sup35NM at 37 °C measured by CLEANEX-PM NMR.

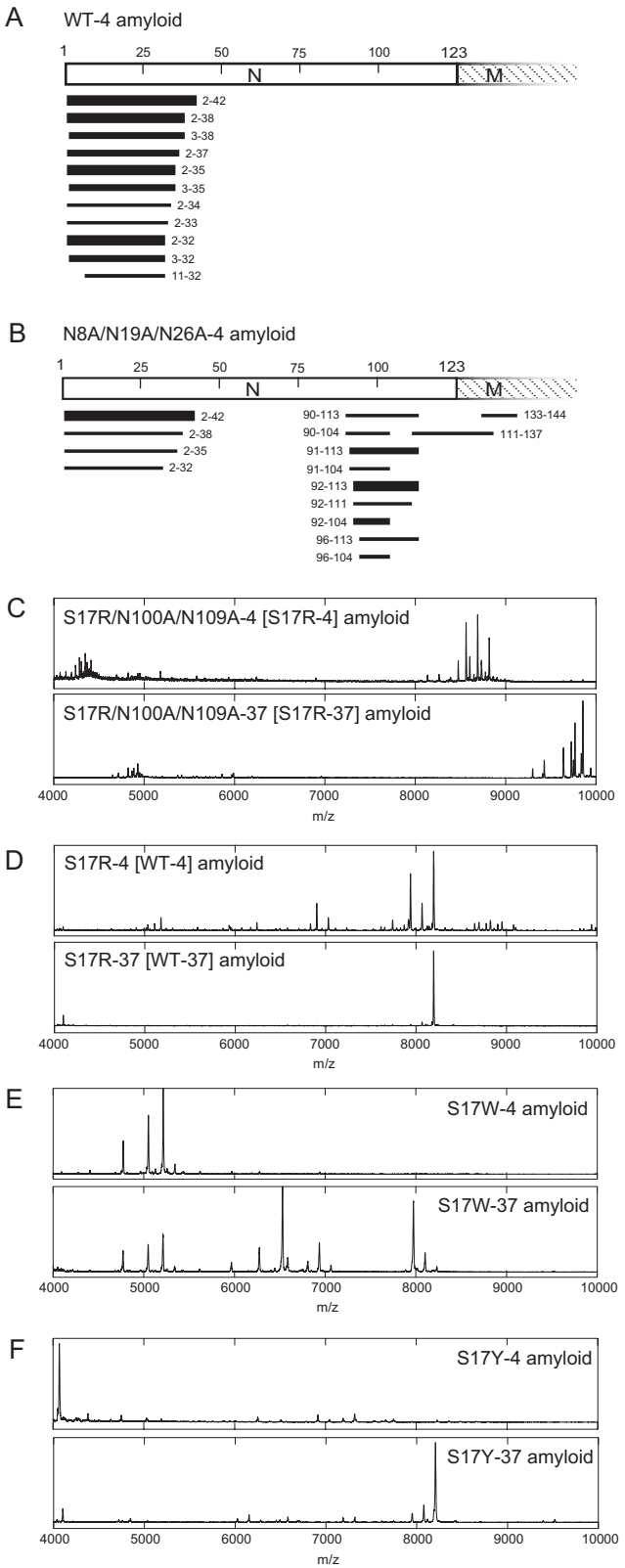

Fig. S6. Amyloid core regions of Sup35NM mutants by mass spectral analysis. (*A*) Core peptides identified in MALDI-TOF/TOF-MS spectra of WT-4 amyloid were aligned to the primary sequence of Sup35NM. The line width is proportional to the signal intensity of peaks in mass spectra. (*B*) Core peptides identified in MALDI-TOF/TOF-MS spectra of N8A/N19A/N26A-4 amyloid were aligned to the primary sequence of Sup35NM. The line width is proportional to the signal intensity of peaks in mass spectra. (*C*) High-*m*/*z*-range MALDI-TOF-MS spectra (*m*/*z* 4,000–10,000) of core peptides derived from S17R/N100A/N109A-4[S17R-4] and S17R/N100A/N109A-37[S17R-37] amyloids. (*D*) High-*m*/*z*-range MALDI-TOF-MS spectra (*m*/*z* 4,000–10,000) of core peptides derived from S17R-4[WT-4] and S17R-37[WT-37] amyloids. (*E*) High-*m*/*z*-range MALDI-TOF-MS spectra (*m*/*z* 4,000–10,000) of core peptides derived from S17W-4 and S17W-37 amyloids. (*F*) High-*m*/*z*-range MALDI-TOF-MS spectra (*m*/*z* 4,000–10,000) of core peptides derived from S17Y-4 and S17Y-37 amyloids.

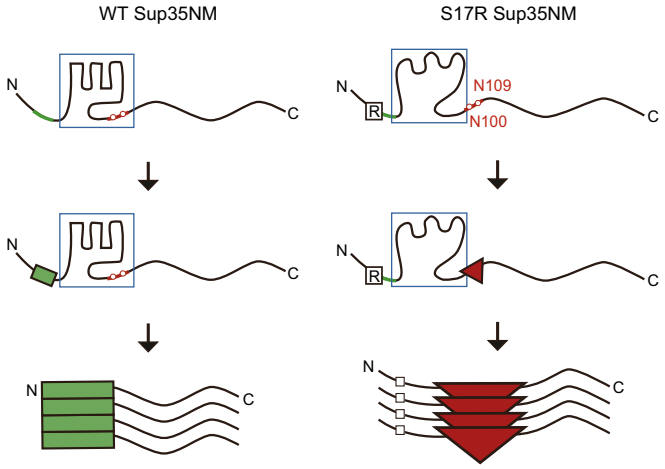

Fig. S7. A proposed model for diversification of Sup35NM amyloid conformation. (*Left*) WT Sup35NM forms a local compact structure (blue box) with buried Asn100 and Asn109, selecting the N-terminal region in the prion domain as an initiation site for amyloid extension (green). (*Right*) By contrast, the S17R mutant shows a relatively unfolded compact structure (blue box). The exposure of Asn100 and Asn109 together with the preference of the S17R mutation not to adopt the N-terminal core results in the selection of PrD-C as an initiation site for amyloid extension (red). The S17R amyloid shows a reduced efficiency in chaperone-mediated fiber fragmentation, which induces the weak/sectoring [*PSI*$^{+}$] strain phenotype.

Table S1. Sup35NM amyloid core peptides identified by mass spectral analysis

Sup35NM amyloid	Fragment, amino acids	Experimental mass, Da	Predicted mass, Da
WT-4	2–38	4,303.5	4,301.2
	2–42	4,671.0	4,668.7
	2–45	4,948.8	4,945.9
	2–46	5,112.3	5,109.1
WT-37	2–70	7,873.7	7,868.9
	2–71	8,001.3	7,997.0
	2–72	8,130.3	8,125.2
S17R-4	82–144	7,187.7	7,184.8
	81–144	7,315.9	7,313.0
	82–147	7,527.9	7,525.3
	82–148	7,615.4	7,612.4
	81–147	7,656.7	7,653.4
	81–148	7,744.3	7,740.5
S17R-37	63–144	9,385.8	9,386.1
	62–144	9,514.8	9,514.2
WT-4 [S17R-4]	82–144	7,189.1	7,184.8
	81–144	7,317.2	7,313.0
	82–147	7,529.2	7,525.3
	82–148	7,616.6	7,612.4
	81–147	7,657.7	7,653.4
	81–148	7,744.8	7,740.5
WT-37 [S17R-37]	63–144	9,387.6	9,386.1
	62–144	9,515.9	9,514.2
S17R-4 [WT-4]	2–61	6,903.1	6,902.0
	2–70	7,938.8	7,938.0
	2–71	8,067.6	8,066.1
	2–72	8,195.4	8,194.3
S17R-37 [WT-37]	2–72	8,194.4	8,194.3
S17R/N100A/N109A-4	2–35	4,059.3	4,057.1
	2–37	4,244.1	4,242.3
	2–38	4,373.0	4,370.4
	2–42	4,740.6	4,737.8
	2–45	5,018.3	5,015.1
	2–46	5,179.9	5,178.3
S17R/N100A/N109A-37	2–70	7,939.1	7,938.1
	2–71	8,067.5	8,066.3
	2–72	8,196.1	8,194.4
S17R/N100A/N109A-4 [S17R-4]	73–148	8,562.1	8,563.4
	72–148	8,690.1	8,691.6
	71–148	8,817.8	8,819.7
S17R/N100A/N109A-37 [S17R-37]	63–147	9,638.9	9,641.5
	63–148	9,726.1	9,728.6
	62–147	9,767.2	9,769.7
	62–148	9,854.0	9,856.7
1M NaCl WT-37	2–46	5,107.8	5,109.1
	2–70	7,865.5	7,868.9
	2–72	8,121.4	8,125.2
	63–144	9,381.0	9,386.1
	62–144	9,509.1	9,514.2
1M NaCl S17R-37	63–144	9,380.1	9,386.1
	62–144	9,508.1	9,514.2
Δ2–34 S17R-4	82–144	7,185.2	7,184.8
	81–144	7,313.3	7,313.0
	82–147	7,525.3	7,525.3
	82–148	7,612.6	7,612.4
	81–147	7,653.5	7,653.4
	81–148	7,741.1	7,740.5
Δ2–34 S17R-37	63–144	9,382.7	9,386.1
	62–144	9,512.3	9,514.2

Table S1. Cont.

Sup35NM amyloid	Fragment, amino acids	Experimental mass, Da	Predicted mass, Da
S17W-4	2–42	4,773.0	4,767.8
	2–45	5,050.6	5,045.0
	2–46	5,214.0	5,208.2
S17W-37	2–55	6,273.9	6,270.4
	2–57	6,530.1	6,526.6
	2–62	6,938.1	6,932.0
	2–70	7,973.1	7,968.0
	2–71	8,102.3	8,096.1
S17Y-4	2–35	4,067.0	4,065.1
S17Y-37	2–70	7,945.4	7,946.0
	2–71	8,073.6	8,074.2
	2–72	8,201.7	8,202.3